

# Molecular shape analysis based upon the Morse-Smale complex and the Connolly function

FRÉDÉRIC CAZALS<sup>1</sup>, FRÉDÉRIC CHAZAL<sup>2</sup> AND THOMAS LEWINER<sup>1,3</sup>

<sup>1</sup> Géométrie Project — INRIA — Sophia Antipolis — France

<sup>2</sup> Department of Mathematics — Université de Bourgogne — France

<sup>3</sup> Department of Mathematics — Pontificia Universidade Católica — Rio de Janeiro — Brazil  
frederic.cazals@inria.fr. fchazal@u-bourgogne.fr. tomlewis@mat.puc--rio.br.

**Abstract.** Docking is the process by which two or several molecules form a complex. Docking involves the geometry of the molecular surfaces, as well as chemical and energetical considerations. In the mid-eighties, Connolly proposed a docking algorithm matching surface *knobs* with surface *depressions*. Knobs and depressions refer to the extrema of the *Connolly function*, which is defined as follows. Given a surface  $\mathcal{M}$  bounding a three-dimensional domain  $X$ , and a sphere  $S$  centered at a point  $p$  of  $\mathcal{M}$ , the Connolly function is equal to the solid angle of the portion of  $S$  containing within  $X$ .

We recast the notions of knobs and depressions in the framework of Morse theory for functions defined over two-dimensional manifolds. First, we study the critical points of the Connolly function for smooth surfaces. Second, we provide an efficient algorithm for computing the Connolly function over a triangulated surface. Third, we introduce a Morse-Smale decomposition based on Forman's discrete Morse theory, and provide an  $O(n \log n)$  algorithm to construct it. This decomposition induces a partition of the surface into regions of homogeneous flow, and provides an elegant way to relate local quantities to global ones —from critical points to Euler's characteristic of the surface. Fourth, we apply this Morse-Smale decomposition to the discrete gradient vector field induced by Connolly's function, and present experimental results for several mesh models.

**Keywords:** *Morse Theory. Differential Geometry. Meshes. Shape Matching. Docking.*

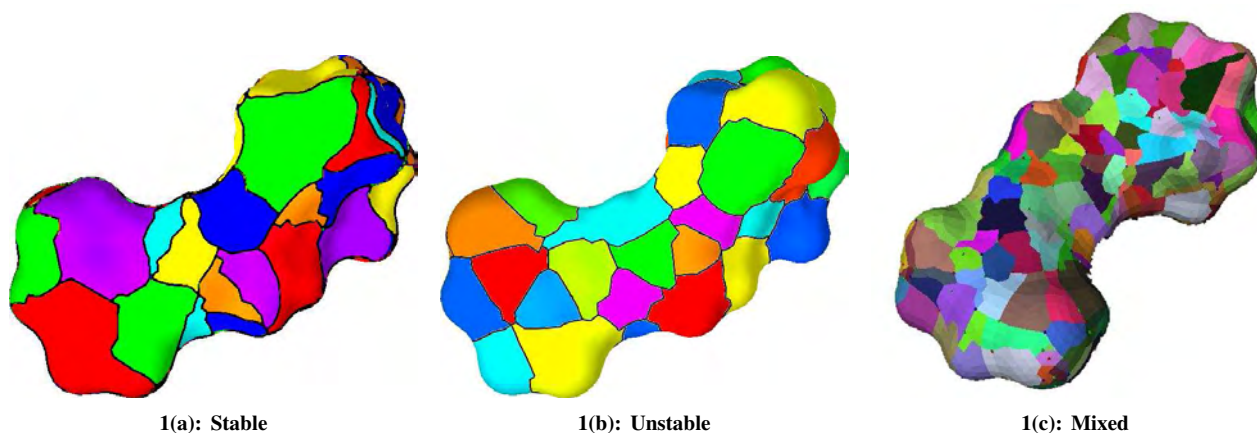


Figure 1: Retinal receptor decomposition.

## 1 Introduction

Docking is the process by which two or several molecules form a complex. These molecular com-

plexes either involve macro-molecules only —DNA, RNA, proteins—, or macro-molecules together with small molecules —typically drugs. The computational study of docking has long been recognized as a major tool to understand biological reactions and to design drugs. Although (bio-)chemist may argue against Connolly that physical and chemical properties play a more prominent role than geometry, geometry is often used as the foundation for

Preprint MAT. 20/02, communicated on December 3<sup>rd</sup>, 2002 to the Department of Mathematics, Pontificia Universidade Católica — Rio de Janeiro, Brazil. The corresponding work was published in the proceedings of the Symposium on Computational Geometry, pp. 351–360, ACM Press, 2003.

a complete approach including chemical and energetic considerations.

When one thinks of docking in terms of geometry, it is appealing to believe that shape complementarity materializes through the pairing of *knobs* and *depressions* of the molecular surfaces —see Figure 2. Knobs and depressions intuitively correspond to local maxima and minima on the surface. But talking of maxima and minima subsumes that (i) a function is defined on the surface (ii) the outputs of the function can be compared —typically a real-valued function. Extrema are then special cases of critical points of the function. Figure 2 features such a function which is a height function. Height functions however are obviously poor candidates for comparing extrema since these depend on the  $z$  direction chosen. Following the idea that critical should be those of a function invariant under rigid motions, Connolly [27, 28] introduced a quantity encoding the portion of a probe sphere centered on the surface and contained within the volume bounded by the surface.

This paper is dedicated to a careful study of Connolly’s function. The first contribution deals with smooth curves and surfaces, while the three others are concerned with triangulated surfaces. Before presenting them, we define precisely Connolly’s function and review some relevant literature.

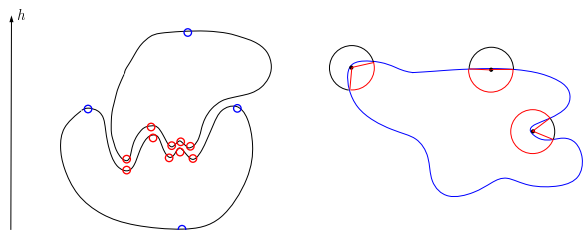


**Figure 2: Complementarity and critical points.**

**Figure 3: The Connolly function for a curve.**

### (a) Probing a surface with Connolly’s function

We begin with the precise definition of Connolly’s function [27, 28]. Let  $X$  be a domain of  $\mathbb{R}^3$  whose boundary  $\mathcal{M}$  is a surface. Let  $S(p, r)$  be a sphere of radius  $r$  centered at a point  $p$  of the surface  $\mathcal{M}$ . Assume that  $r$  is small enough so that  $\mathcal{M}$  cuts  $S$  into two two-dimensional topological disks  $D_i$  and  $D_o$  —the subscripts respectively stand for inside and outside  $X$ . The Connolly function is defined as the solid angle associated with  $D_i$ , that is:

$$C(p, r) = \frac{\text{SurfaceArea}(D_i)}{r^2}. \quad (1)$$

The Connolly function therefore maps a point of the surface to a real value within the interval  $]0, 4\pi[$ . Notice that a similar definition holds for curves using a circle instead of a sphere. The intuition behind Connolly’s function is illustrated on Figure 3 with a curve for which three probing

circles have been depicted. From left to right, they respectively correspond to a peak, a flat area, and a depression of the curve. Over these three configurations, the Connolly function takes an increasing value, and the initial incentive for defining such a function was “the sharper the peak, the smaller the value; the more depressed the crevice, the higher the value”.

The previous definition does not assume anything about the geometry of  $\mathcal{M}$ . For example, domain  $X$  could be defined by a set of equations —e.g. a semi-algebraic set, or could have a more combinatorial description —e.g. a union of Van der Waals balls representing the atoms of a molecule. We shall in this paper carry out a general study of the Connolly function and in particular of its critical points for (i) smooth surfaces (ii) triangulated surfaces. Although the definition of Connolly’s function stems from a focus on molecular modeling, our investigations are independent from the physical meaning of the surface studied. The last section however, deals with molecular solvent-accessible triangulated surfaces [25].

### (b) Previous work

Our review of previous work discusses in turn (i) contributions dealing with the definition of a function on a molecular surface (ii) Morse Theory (iii) contributions concerned with the global characterization of molecular features. We focus on the geometric aspects and do not discuss in depth the underlying implications for applications. See e.g. [18, 20] for recent references on docking.

**Functions defined over molecular surfaces** The Connolly function was first introduced to study docking [27, 28]. The initial idea was to seek local extrema of the function and to match maxima with minima. For a real valued function of two variables, local maxima and minima, together with saddle points, the so-called critical points. More precisely, any function of two variables whose Hessian is non degenerate at a critical point can be re-written, up to a diffeomorphism, as a local maximum, minimum, or saddle [22]. Connolly, however, points out that saddle points are difficult to deal with [28, p1236] “saddle points have not proven to be useful in docking because too many critical points over-complicate matters”. Refinements of Connolly’s algorithm [29, 30] do not use the information provided by saddle points neither.

An interesting docking algorithm implicitly using critical points is described in [34]. Star-shaped molecules can be modeled using spherical harmonics. The molecular surface is then defined as the graph of a function of two variables  $r(\theta, \varphi)$ . The contour map of this height function is used to define a fingerprint of the surface. The topology of the contour map naturally involves the critical points of the height function since contour lines are integral curves for the vector field  $(\partial r / \partial \varphi, -\partial r / \partial \theta)$ .

**Morse Theory and dynamical systems** The subject of critical points naturally calls for Morse Theory [24] and dynamical systems [31]. Critical points of a Morse function defined on a manifold can be used to partition the manifold into regions of homogeneous flow [9], the so-called stable and unstable manifolds. The intersection of stable and unstable manifolds defines the Morse-Smale complex. An algorithm computing the Morse-Smale complex of a function defined on a piecewise linear surface by mimicking the smooth setting has been introduced in [15].

In addition to the *smooth* Morse theory just mentioned, a combinatorial Morse theory [1, 2] has been developed recently. Discrete gradient vector fields actually underly our Morse-Smale decomposition algorithm. A decomposition algorithm based on a flow diagram for the particular case of disks in the plane is presented in [17].

**Global molecular properties** Connolly's contribution discussed so far is mainly concerned with local geometric features. More global analysis are concerned with the characterization of voids—that is regions of a macro-molecule not accessible from the outside, as well as cavities—that is excavations with a small opening on the outside. The reader is referred to [14] for algorithms reporting voids and cavities based upon weighted Voronoi diagrams. An interesting source of information for global characterization of molecular properties is also [32].

In a different application area, namely that computer vision, and for the particular issue of characterizing human faces, the reader is referred to [19]. This book indeed provides several methods for characterizing patterns of the face.

### (c) Contributions and paper overview

We are now ready to state more precisely the contributions of this paper:

- First, we investigate Connolly's function for smooth curves and surfaces. The incentive for such a study is to relate the critical points of the function to differential quantities of the surface and in particular extrema of principal curvatures along curvature lines—refer again to [19, 21].
- Second, we provide an efficient algorithm to compute Connolly's function over triangulated surfaces.
- Third, we introduce the notion of discrete Morse-Smale decomposition based upon a discrete gradient vector field [1, 2]. This decomposition bridges the gap between local quantities—the critical points—and the global geometry of the triangulated manifold. This decomposition is more natural for triangulated surfaces than the one presented in [15], and can be computed in  $O(n \log n)$  time.
- Fourth, we apply the previous Morse-Smale decomposition to the discrete gradient vector field induced

by Connolly's function, and present experimental results for several molecules as well as standard computer graphics models.

## 2 The Connolly function for smooth curves and surfaces

Spherical caps on van der Waals balls, or triangles contributing to a piecewise linear surface are not the most accurate primitives to model molecular surfaces. For example, spherical harmonics or electron density contours [25] provide smooth models for such surfaces. In this section, we investigate some properties of the Connolly function for smooth i.e. infinitely differentiable surfaces. As a preliminary step, we examine the case of curves. The conclusions we are heading over are twofold: for small values of the probe sphere radius, the critical points of Connolly's function are nearby extrema of curvature for curves, and nearby critical points of the mean curvature function for surfaces.

From a differential geometry perspective, a difficulty with Connolly's function is that it is not just local—as opposed to the curvature for example. For the case of curves, these global interactions can be managed through explicit differential equations—as opposed to mere Taylor expansions for surfaces.

### (a) The Connolly function for smooth curves

Let  $\mathcal{C}$  be a smooth compact curve in  $\mathbb{R}^2$  and let  $\gamma(s)$  be a parameterization of  $\mathcal{C}$  by arc length—see Figure 4. The Frenet frame and the curvature of  $\mathcal{C}$  at  $s$  are respectively denoted  $(T(s), N(s))$  and  $\kappa(s)$ . Let  $\eta$  be a positive real number so that the circle of radius  $\eta$  centered at  $\gamma(s)$  intersects the curve  $\mathcal{C}$  in two points  $\gamma(t^+(s))$  and  $\gamma(t^-(s))$ , with  $t^-(s) < s < t^+(s)$ . Let  $u^+(s)$  and  $u^-(s)$  be the unitary vectors defined by:

$$u^+(s) = \frac{\gamma(t^+(s)) - \gamma(s)}{\eta}, \quad u^-(s) = \frac{\gamma(t^-(s)) - \gamma(s)}{\eta}.$$

We denote by  $\theta^+(s)$  (resp.  $\theta^-(s)$ ) the oriented angle between  $\gamma'(s)$  and  $u^+(s)$  (resp.  $u^-(s)$  and  $-\gamma'(s)$ ):

$$\theta^+(s) = \widehat{\gamma'(s), u^+(s)} \quad \text{and} \quad \theta^-(s) = \widehat{u^-(s), -\gamma'(s)}.$$

At point  $\gamma(s)$ , the Connolly function  $C(s)$  is defined by the length of the circle arc from  $\gamma(t^-(s))$  to  $\gamma(t^+(s))$  normalized by  $\eta$ , or equivalently by the angle:

$$C(s) = \pi + \theta^+(s) + \theta^-(s). \quad (2)$$

The aim of this section is to study Connolly's function for fixed radius  $\eta > 0$ .

The configurations for the two intersection points are similar and can be investigated at once. Therefore, let  $\varepsilon$  take the value  $+$  ( $-$ ) if  $\gamma(t^+(s))$  ( $\gamma(t^-(s))$ ) is concerned. The following lemma can be proved:

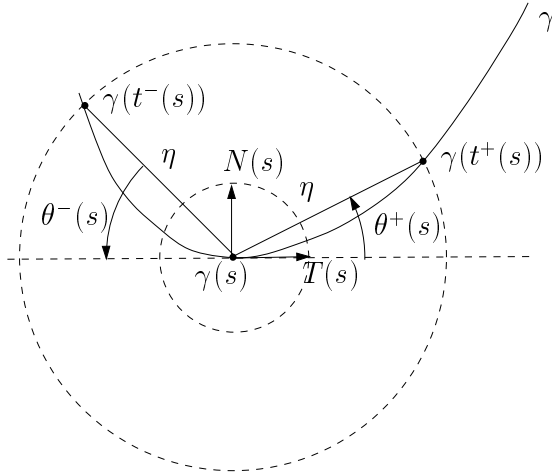


Figure 4: Connolly function for a curve: notations

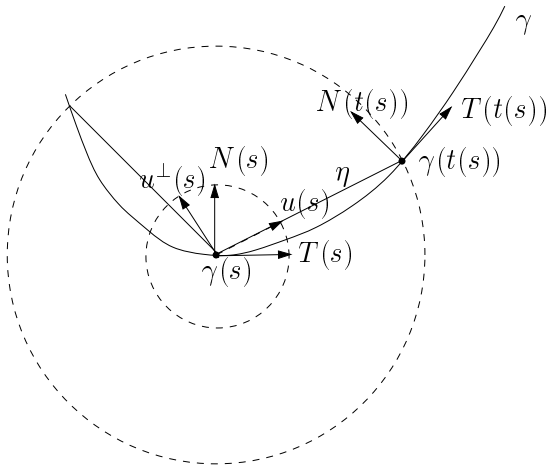


Figure 5: Differential Eq. for  $\theta(s)$ : notations

**Lemma 1** For a fixed arc-length value  $s$ , one has :

$$t(s, \eta) = s + \varepsilon\eta + o(\eta^2), \quad (3)$$

$$\frac{\partial \theta}{\partial s}(s, \eta) = \varepsilon \langle \gamma^{(3)}(s) | \gamma'(s)^\perp \rangle \frac{\eta}{2} + o(\eta) = \frac{1}{2} \frac{d\kappa}{ds}(s) \eta + o(\eta). \quad (4)$$

This lemma helps to localize the critical points of Connolly's function. If  $s$  is such that the curvature of curve  $\mathcal{C}$  at point  $\gamma(s)$  is regular, then for  $\eta$  sufficiently small, Connolly's function is also regular at  $\gamma(s)$ . Hence for  $\eta$  small, critical points of Connolly function are located in a neighborhood of critical points of the curvature. This coincides with the intuition that the extrema of Connolly's function are located near the extrema of curvature of  $\mathcal{C}$ .

More precisely, let  $Sing(\kappa) = \{\gamma(s) : \kappa'(s) = 0\}$  be the critical set of the curvature function  $\kappa(s)$  and let  $Sing(C, \eta) = \{\gamma(s) : C'(s, \eta) = 0\}$  be the set of critical

points of the Connolly function corresponding to radius  $\eta$ . If  $A$  and  $B$  are two subset of the plane, denote by

$$\mathcal{H}(A|B) = \sup_{m \in A} d(m, B)$$

the one sided Hausdorff distance between  $A$  and  $B$ , where  $d(\cdot, B)$  is the Euclidean distance to  $B$ . Remind that  $\mathcal{H}(\cdot)$  is not a distance between sets : it is not symmetric and  $\mathcal{H}(A|B) = 0$  does not imply  $A = B$ . We have:

**Theorem 2** With previous notations one has

$$\lim_{\eta \rightarrow 0} \mathcal{H}(Sing(C, \eta) | Sing(\kappa)) = 0.$$

### (b) The Connolly function for smooth surfaces

Consider now the Connolly function given by equation (1) assuming  $\mathcal{M}$  is a  $C^\infty$  compact surface embedded in  $\mathbb{R}^3$ . Let  $p$  be a point of  $\mathcal{M}$ . Denote  $\kappa_1, \kappa_2$  and  $H$  the principal and mean curvatures of  $\mathcal{M}$  at  $p$ . Also, let  $A(p, \eta)$  stand for the surface area of the sphere  $S(p, \eta)$  contained within the volume bounded by  $\mathcal{M}$ . We first generalize lemma 1 to the case of surfaces.

**Lemma 3** There exists a  $C^\infty$  function  $\varepsilon$  defined on  $S \times \mathbb{R}_+$  such that

$$C(p, \eta) = \frac{A(p, \eta)}{\eta^2} = 2\pi + \pi H(p)\eta + \eta^2 \varepsilon(p, \eta) \quad (5)$$

with  $\lim_{\eta \rightarrow 0} \varepsilon(p, \eta) = 0$ .

Note that in the proof of lemma 3 we use [33, Lemma 1] instead of results obtained previously for curves. It is here more convenient to work with parameterization  $(t, g_\theta(t))$  for  $\mathcal{M}_\theta$  instead of arc-length parameterization.

As in the case of curves, previous lemma allows to localize the critical points of the Connolly function using the one sided Hausdorff distance. Let  $\nabla H(p)$  be the gradient of function  $H$  at point  $p$  and,  $\eta$  being fixed, let  $\nabla C(p, \eta)$  be the gradient of Connolly function  $C$  at point  $p$ . One has:

**Theorem 4** Let  $Sing(H) = \{p \in \mathcal{M} : \nabla H(p) = 0\}$  be the critical set of the mean curvature function  $H$  and let  $Sing(C, \eta) = \{p \in \mathcal{M} : \nabla C(p, \eta) = 0\}$  be the critical set of the Connolly function corresponding to radius  $\eta$ . One has

$$\lim_{\eta \rightarrow 0} \mathcal{H}(Sing(C, \eta) | Sing(H)) = 0.$$

As an illustration of the previous Theorem, Figure 6 provides a visual comparison of Connolly's function versus the mean curvature, whose evaluation can be performed from a mesh with either provably good algorithm [16, 12].

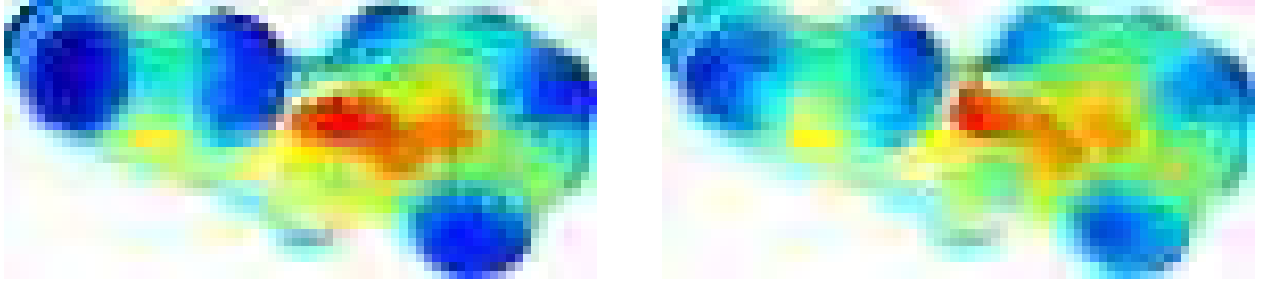


**Figure 6: Connolly function  $(C - 2\pi)/(\pi \cdot r)$  (left) versus mean curvature (right) on a molecular surface. Color scales are mapped from  $-0.746 \dots 0.466$  (left) and from  $-0.877 \dots 0.663$ .**

**Relationship to ridges** Important curvature properties of surfaces are encoded by ridges, that is extrema of principal curvature along curvature lines [10, 21]. For example, points located on elliptic ridges may be the contact points of maximal spheres contributing to the skeleton—but not the medial axis— of the complement  $\mathbb{R}^3 \setminus \mathcal{M}$  of  $\mathcal{M}$ . correspond to maximal spheres with a single contact point to  $\mathcal{M}$ , that is their centers lie of the skeleton associated with the complement of  $\mathcal{M}$ —but not on its medial axis.

As pointed out in introduction—refer again to Figure 3, Connolly’s function is obviously related to curvature properties. As just proved, the critical points of Connolly’s function are located nearby critical points of the mean curvature function  $H$ . We therefore take a quick look at the exact relationship between critical points of  $H$  and ridges.

Consider the expression of surface  $\mathcal{M}$  as a height function near point  $p$ . More precisely, express this height function in the coordinate system associated with the principal directions and whose  $z$  axis is the normal to  $\mathcal{M}$  at  $p$ —this is the so-called Monge form of the surface. The following lemma is a straightforward application of [11, p.439], and shows that the critical points of  $H$  do not lie on ridges since required conditions there are  $a = 0$  or  $d = 0$ :

**Lemma 5** Assume the Monge form of the surface  $\mathcal{M}$  at  $p$  is given by

$$f(x, y) = \frac{1}{2}(\kappa_1 x^2 + \kappa_2 y^2) + \frac{1}{6}(ax^3 + 3bx^2y + 3cxy^2 + dy^3) + \dots$$

Then, the local expansion of the mean curvature  $H$  satisfies

$$2H(x, y) = \kappa_1 + \kappa_2 + (c+a)x + (b+d)y + \|(x, y)\|\delta(x, y)$$

with  $\lim_{(x,y) \rightarrow 0} \delta(x, y) = 0$ .

*Proof:* Recall that

$$H = \frac{f_{yy}(1 + f_x^2) - 2f_x f_y f_{xy} + f_{xx}(1 + f_y^2)}{2(1 + f_x^2 + f_y^2)^{\frac{3}{2}}}$$

(see for example [11, p.439]) where  $f_x, f_y, f_{xx}, f_{yy}$  and  $f_{xy}$  are the first and second order partial derivatives of  $f$ . We have:

$$\begin{aligned} f_x &= \kappa_1 x + o(x, y), \\ f_y &= \kappa_2 y + o(x, y), \\ f_{xx} &= \kappa_1 + 6ax + 2by + o(x, y), \\ f_{yy} &= \kappa_2 + 2cx + 6dy + o(x, y), \\ f_{xy} &= 2bx + 2cy + o(x, y). \end{aligned}$$

Expansion of  $H$  results easily from previous equalities. ■

### 3 Computing the Connolly function for a mesh

This section presents the calculation of the Connolly function defined by equation (1) for a triangulated surface  $\mathcal{M}$ . We assume the surface is represented by a halfedge data structure [23]. The sphere of radius  $r$  centered at a vertex  $p$  of the mesh is denoted  $S(p, r)$ .

**Outline** Consider the sphere  $S(p, r)$ . If  $r$  is small enough, the surface  $\mathcal{M}$  cuts  $S$  into two topological disks, one of which entirely lies within the volume bounded by  $\mathcal{M}$ . The intersections between the triangles of the mesh and  $S$  consist of circle arcs. Such an arc is a great circle arc if the plane of its defining triangle contains the center of  $S$ , and a small circle arc otherwise. Let  $C = \{C_1, \dots, C_k\}$  be the set of circle arcs. As observed in [27], the local Gauss-Bonnet theorem can be invoked to compute the surface area of the patch we are interested in.

To see how, orientate the intersection curve  $C$  so as to leave to the left the interior of the patch we want to compute the area of. Also, let  $\Delta\theta_i$  be the tangent turn between the endpoint of  $C_i$  and the starting point of  $C_{i+1}$ . Also denote  $k_g$  the geodesic curvature. The local Gauss-Bonnet theorem states that

$$\sum_i \Delta\theta_i + \sum_i \int_{C_i} k_g ds + \frac{1}{r^2} Area = 2\pi, \quad (6)$$

from which the surface area is easily derived if the  $\Delta\theta_i$ s and the geodesic curvatures are known.

**Computing the intersection curve  $C$**  To report the intersections between the triangles of the mesh and the sphere  $S$ , we proceed by first finding an edge  $h_0$  crossing the sphere  $S$ , and second by walking along the intersection curve  $C$  from the triangles incident to  $h_0$ . Notice that each triangle edge intersects  $S$  in at most two points, so that the intersection of a triangle with the probe sphere consists of at most six points. Figure 8 depicts the three possible intersection configuration between a triangle and  $S$ . Triangles  $T$ ,  $F$  and  $W$  respectively intersect  $S$  in two, four, and six (worst-case) points.

More precisely, let  $h_0$  be a halfedge crossing  $S$ . Let  $T$  be a triangle incident to  $h_0$  and denote  $\{h_0, h_1, h_2\}$  its edges. The intersection between  $T$  and  $S$  is one of the two configurations depicted on Figure 8—that is the second intersecting edge is either  $h_1$  or  $h_2$ . Therefore, once a starting edge  $h_0$  has been found, one just needs to find the second intersected edge of the triangle under consideration, move into the adjacent triangle, and iterate.

The key issue consists of finding  $h_0$ . Let  $v$  be the vertex where the probe sphere is centered. A naive strategy is to (i) select the farthest neighbors  $p$  of  $v$  (ii)check whether the edge  $vp$  crosses  $S$  (iii)if not, iterate the *farthest neighbor of  $v$  from  $p$*  until a crossing edge has been found. This strategy may lead to a deadlock for big probe spheres, in which case an exhaustive search of the neighboring graph anchored at  $v$  can be performed.

**Computing the angle turns  $\Delta\theta_i$**  Computing the angle turns  $\Delta\theta_i$ s requires the knowledge of the tangents at the endpoints of the circle arcs  $C_i$ s. We therefore seek a parameterization of these circle arcs.

Consider a triangle  $T$ , two edges of which intersect  $S$ . Let  $p_1$  and  $p_2$  be the intersection points of these two edges with  $S$ , and let  $c$  be the center of the corresponding circle arc—see Figure 9. The line-segment  $p_1p_2$  is parameterized by  $X(t) = (1 - t)p_1 + tp_2$ ,  $t \in [0, 1]$ . Assuming no triangle is degenerate—i.e. has an angle equal to  $\pi$ ,  $X(t)$  can be uniquely scaled so as to lie on  $S$ . Let  $L(t)$  be the parameterization sought. If  $r_c$  denotes the radius of the small circle, i.e.  $r_c = |cp_1|$ , we have:

$$cL(t) = r_c \frac{cX(t)}{|cX(t)|},$$

from which the tangent vector at any point of the circle arc is derived.

**Computing the geodesic curvatures** The last step required to evaluate the surface area from the local Gauss-Bonnet theorem is to compute the geodesic curvatures  $k_g$  along the circle arcs. Denote  $d_c$  the distance between the sphere center and the small circle center,  $r$  the radius of  $S$ ,

and  $r_c$  the small circle radius. As noticed in [27], the absolute value of  $k_g$  is given by  $k_g = d_c/(r r_c)$ . However, this does not give the sign of  $k_g$ .

We therefore resort to the definition of the geodesic curvature based upon the covariant derivative [26]. Let  $\gamma$  be a curve parameterized by arc length on a smooth surface. Denote  $\gamma'(s) = t(s)$  the tangent vector and  $\gamma''(s) = dt/ds = kn$  be the curvature vector of  $\gamma$ . Also, let  $N$  stand for the normal of the surface. The geodesic curvature is defined by the covariant derivative of the tangent vector  $t$ , i.e.

$$k_g = \left[ \frac{d\gamma'}{ds} \right] = \left\langle \frac{d\gamma'}{ds}, N \wedge \frac{d\gamma'}{ds} \right\rangle = \langle kn, N \wedge t \rangle .$$

For a small circle, the latter formula is especially convenient since  $kn$  points to the center  $c$  of the small circle, and has magnitude  $1/r_c$ .

## 4 Constructing a discrete Morse–Smale decomposition

We aim to analyze a scalar field  $f$  defined at the vertices of a mesh. In particular, we want to decompose the domain of  $f$  into patches where the flow of  $f$  is uniform. In the smooth case, this decomposition has been introduced by Thom [9] and Smale [6] based on Morse theory [24]. Although an algorithm for computing quasi–Morse complexes already exists [15], the algorithm introduced here is simpler, faster. It does not follow the *simulation of differentiability* paradigm, and is therefore more natural for combinatorial surfaces.

It is based upon Forman’s Morse theory [2], a discrete version of Morse theory. This theory extends the classical Morse theory to cell complexes, relating the topology of such a structure to the study of functions defined on it. The cell complex structure is particularly well suited for the study of meshes, and allows direct computations with a strong theoretical framework. Since Forman’s Morse theory is combinatorial, it does not require any approximation. The algorithm following our analysis is simple and accommodates a hierarchy, which can be used to remove topological noise.

We shall prove that Connolly’s function is admissible for the discrete framework, and show how the hierarchy can be used to get rid of useless patches when the radius of the Connolly ball is not adapted.

### (a) Smooth Morse–Smale decomposition

Given a smooth 2–manifold  $M$  and a smooth map  $f : M \rightarrow \mathbb{R}$  defined on it, an *integral curve* is a curve whose velocity vector everywhere matches the gradient  $\nabla f$  of  $f$ . The *critical points* are the points where the gradient vanishes. The *stable manifold* of a critical point  $c$  is the union of all the integral curves converging to  $c$ . The *unstable mani-*

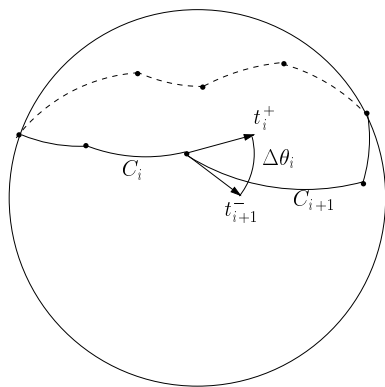


Figure 7: Gauss-Bonnet on a spherical cap.

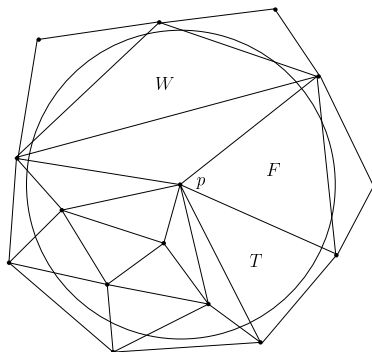


Figure 8: Walking around the intersection curve.

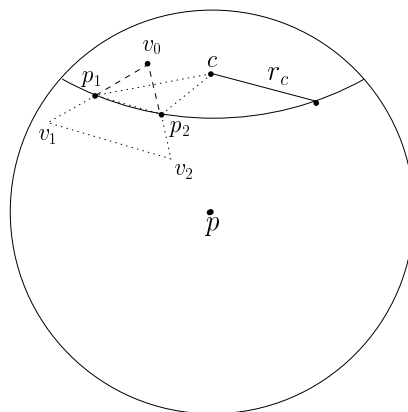


Figure 9: Parameterizing a small circle.

fold of a critical point  $c$  is the union of all the integral curves originating from  $c$ .

A function is *Morse-Smale* if its critical points are non-degenerate and if its integral curves cross transversally. It has been proven in [15, Lemma 1] that the intersections of the stable and unstable manifolds form a cell complex, where each 2-cell is a quadrangle with critical vertices of index 0,1,2,1 in this order around the region. This property characterizes a *quasi Morse complex*. The decomposition introduced here also has this property.

### (b) Forman's discrete Morse theory

The building block of Forman's theory is the *discrete gradient vector field*. It corresponds to the gradient of a smooth Morse function. The discrete gradient vector field is equivalent to discrete Morse functions, as proved in [2].

A *combinatorial vector field*  $\mathcal{V}$  defined on a manifold is a collection of disjoint pairs of incident cells: vertex/edge, edge/face,...

A  $\mathcal{V}$ -path is an alternating sequence  $\alpha_0, \beta_0, \alpha_1, \beta_1, \dots$  of cells such that:

- all the cells  $\alpha_i$  are of the same dimension  $p$ , and all the cells  $\beta_i$  are of the same dimension  $p + 1$ .
- $\alpha_i$  and  $\beta_i$  are incident cells, and so are  $\beta_i$  and  $\alpha_{i+1}$ .
- the pairs  $\{\alpha_i, \beta_i\}$  are elements of the vector field  $\mathcal{V}$ .

A *discrete gradient vector field* is a combinatorial vector field with no non-trivial closed  $\mathcal{V}$ -path.

Morse proved that the topology of a manifold is related to the critical elements of a smooth function defined on it. Forman gave an analogous result, with the following definition for the critical cells: a cell is *critical* if it is not paired with any other cell.

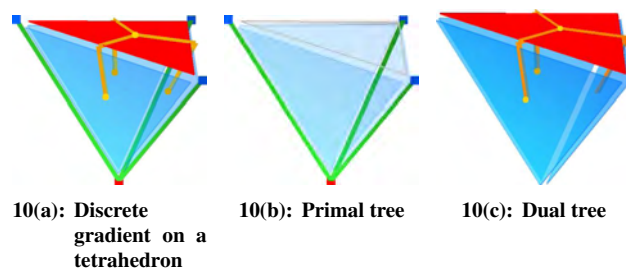


Figure 10: (a) A discrete gradient vector field on a tetrahedron: 1 critical vertex, 1 critical face (in red) (b),(c) The corresponding primal and dual rooted trees

### (c) Discrete gradient vector fields and rooted forests

It has been proven in [4, 5] that a discrete gradient vector field on a closed 2-manifold is in fact a pair of *interlaced primal and dual rooted spanning forests*. The dual graph  $D$  of a closed 2-manifold  $M$  represents each face of  $M$  by a node, and the edges of  $M$  by a link joining adjacent nodes. A dual spanning forest  $DF$  of  $M$  is a subgraph of  $D$  with no cycle, containing all the nodes of  $D$ . A rooted forest has one node distinguished as the root for each connected component. A discrete gradient vector field on  $M$  is equivalent to a primal and a dual spanning forests  $PF$  and  $DF$  such that (i) all vertices of  $M$  are represented in  $PF$ , all faces in  $DF$  and (ii) an edge of  $M$  is not represented in both  $DF$  and  $PF$  — it is possible that an edge is represented neither in  $DF$  nor in  $PF$ . For example, Figure 10(b) and Figure 10(c) show the primal and dual trees of the discrete gradient vector field of Figure 10(a).

The critical vertices (minima) are the roots of the primal forest, the critical faces (maxima) are the roots of the dual forest and the critical edges (saddles) are the edges that belong neither to the primal nor to the dual forest. For example, Figure 11(a) and Figure 11(b) shows the interlaced

forest and their critical points on a small sphere with saddle model.

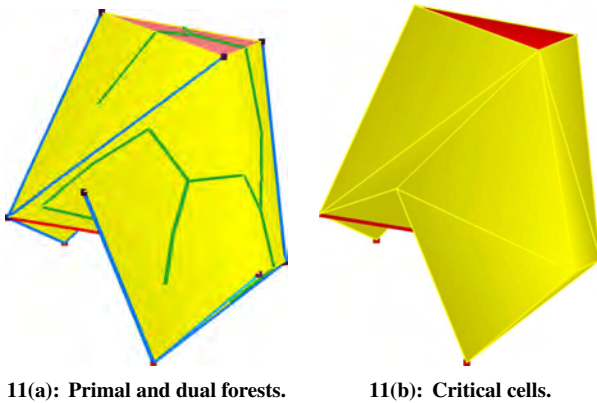


**Figure 11:** (a) The interlaced primal (green) and dual (orange) forests. (b) One maximum (top triangle), two minima (bottom-most vertices) and one saddle (horizontal edge).

#### (d) Discrete decomposition

##### Discrete stable and unstable regions

The discrete gradient vector field points on the primal forest from the roots to the leaves, and in the dual tree from the leaves to the roots. Therefore, an integral curve is of two kinds: a  $\mathcal{V}$ -path formed by vertices and edges, or a  $\mathcal{V}$ -path formed by faces and edges.

The stable region of a maximum (face) is its component in the dual forest. The unstable region of a minimum (vertex) is its component in the primal forest. The stable region of a minimum and the unstable region of a maximum are reduced to themselves (as in the smooth case). Notice that, as a difference with the smooth case, the stable and unstable regions are defined on different elements: the stable region is defined on faces, and the unstable one on vertices.

##### Discrete Morse–Smale decomposition

The Morse–Smale decomposition is usually computed by intersecting the stable and unstable regions, creating *patches*. As in our case they rely on separate cells, this cannot be done directly. A stable region can be extended to manifold by including all its inner edges and vertices. The edges and vertices on the boundary of the region will be the boundary of the manifold. An unstable region can be extended to a 2-manifold by including all the triangles with all its vertices in the unstable region. The boundary is then a set of faces. It can be left empty, be attributed to both bounding regions (overlapping boundary), which could be suitable for docking applications. We can also attribute each face to the region that contains most of its vertices, starting from the saddle points (adapted boundary). Figure 12(a) shows the result on a figure-eight-knot model.

The property of quasi Morse complex remains for closed 2-manifolds: minima and maxima cannot be connected, as the primal and dual forests are disjoint. For the same reason, a saddle cell cannot be connected to another saddle. Therefore, the boundary of every patch of the discrete Morse–Smale decomposition is composed of sequences of minimum, saddle, maximum and saddle. One patch corresponds to the intersection of the tree component of a maximum with the tree component of a minimum. Therefore, it cannot contain more than one minimum, and its boundary consists of only one sequence minimum, saddle, maximum, saddle.

##### A discrete gradient vector field from Connolly’s function

Defining a smooth Morse function on a mesh based on a scalar field usually requires that the values of the scalar field on the vertices are all different. This can be obtained by a small perturbation, and ensures the uniqueness of the Morse–Smale decomposition. Then, the function is interpolated on the edges and faces of the mesh to comply theoretically with the requirements of a Morse function.

The theoretical framework of Forman’s theory gives a more straightforward justification. A discrete gradient vector field on a closed 2-manifold is equivalent to interlaced forests such that, on each component of the forest, the discrete gradient is monotone along the edges from the leaves to the root [4]. Any scalar field  $f$  given on the vertices of a mesh can also be decomposed into primal trees where  $f$  is monotone. The dual trees are obtained in a similar way by assigning to each face the mean value of its vertices. (To avoid having more maximal faces than the number of maxima of  $f$ , this argument is refined in the algorithm.) Therefore, any scalar field defined on the vertices can be completed to a discrete gradient vector field (which is equivalent to a discrete Morse function [2]). This completion is unique when the scalar field is injective.

##### Decomposition algorithm

Given a function  $f$  on every vertex, the algorithm proceeds in four steps. Each cell (vertex, edge, face) has an extra pointer to store the patch structure (the union/find structure [7]) for vertices and faces, and to mark as visited for edges. The algorithm computes first the stable regions, and then the unstable ones.

1. It identifies the local minima and the local maxima, by comparing the value of  $f$  on a vertex to the value of  $f$  on each of its adjacent vertices.
2. The dual spanning forest is built, with the maxima of  $f$  as roots (remind that in the dual setting, values of  $f$  refer to values of  $f$  over the facets, and that edges actually connect two facets). The classical algorithm for minimal spanning tree [8] is used in the following manner. The edges are processed by increasing value

(mean value of their incident vertices). When testing if an edge joins two different components, using the union/find data structure, it does not select an edge that would join two trees with different maxima. Otherwise, the edge is selected and marked as visited, and the union/find structure is updated. Therefore, we get a face-spanning forest, with one component per maxima. This maximum will be used as the root of the component.

3. It builds the primal spanning forest, with the minima of  $f$  as roots, in the same way as at the second step (processing the edges in a reverse order).
4. It computes the intersection of the stable and unstable regions, by marking the edges of each region with a different identifier. It uses a dictionary to store the pair unstable/stable identifier of each patch (with lexicographic key). The different options for the extension of the stable manifold, i.e. empty boundary, overlapping boundary and adapted boundary are given as an optional argument.

The algorithm's complexity is  $O(n \log(n))$  for the edge sorting, and  $O(n\alpha(n))$  for the forest creation, where  $n$  denotes the size of the mesh and  $\alpha(n)$  is the inverse of Ackerman's function. At the end of the algorithm, each vertex and each face carries its patch number (as a union/find structure). For faces [resp. vertices], this denotes the stable [resp. unstable] region it belongs to. In the algorithm, we only care about the minima and the maxima. We know the Euler characteristic can be expressed as the alternated sum of the critical cells, or equivalently of all the cells. This guarantees we did not create any meaningless saddle critical cell.

### Smale's order and Noise removal

Critical cells correspond to local maxima, minima and saddles. Therefore, a small perturbation of the scalar field would create a critical cell that would perturb the overall readability of the result. It would be convenient to rate each critical cell by its contribution to the overall scalar field, and to be able to cancel meaningless critical cells.

Forman's theory allows a very easy computation of a cancellation. If we want to cancel a minimum (resp. maximum)  $m$  with a saddle  $s$  incident to the tree component of  $m$  in the primal (resp. dual) forest, it is sufficient to add this saddle to the primal (resp. dual) forest. This is possible only if it does not create cycle, i.e. if the saddle  $s$  is also incident to a different tree component of the primal (resp. dual) forest. This is equivalent to computing the whole decomposition, removing  $m$  from the list of local minima (resp. maxima). From the computational side, it is just a union in the union/find structure.

The hierarchy can be obtained by the Smale's order: a critical cell  $c_1$  is inferior to a critical cell  $c_2$  if the unstable region of  $c_1$  intersects the stable region of  $c_2$ . This partial order can be represented as a graph. This graph is easily built by looking at which maxima and minima the saddles would join. We see on Figure 12(b) that this graph points out the quasi-Morse complex property of the decomposition.

Consider a minimum-saddle cancellation  $C$ . For a possible cancellation  $C$ , denote  $\delta(C)$  the difference of the scalar field at the two critical cells.  $C$  is possible if the saddle is connected with another minimum. Therefore, the saddle can be canceled in two ways, with both minima. The natural option is the cancellation with the smaller  $\delta$ . It is now possible to order the possible cancellations by their  $\delta$ , and to cancel each pair that is below a given threshold. This is actually equivalent to the hierarchy introduced in [15].

The possible cancellations of Figure 12(b) are v0/s2, v1/s2, v0/s3, v1/s3, s0/f0, s0/f1, s1/f0, s1/f1. The figure is graduated with the value of scalar field  $f$ . Thus, we can read the most likely cancellations: v1/s2 and s1/f0.

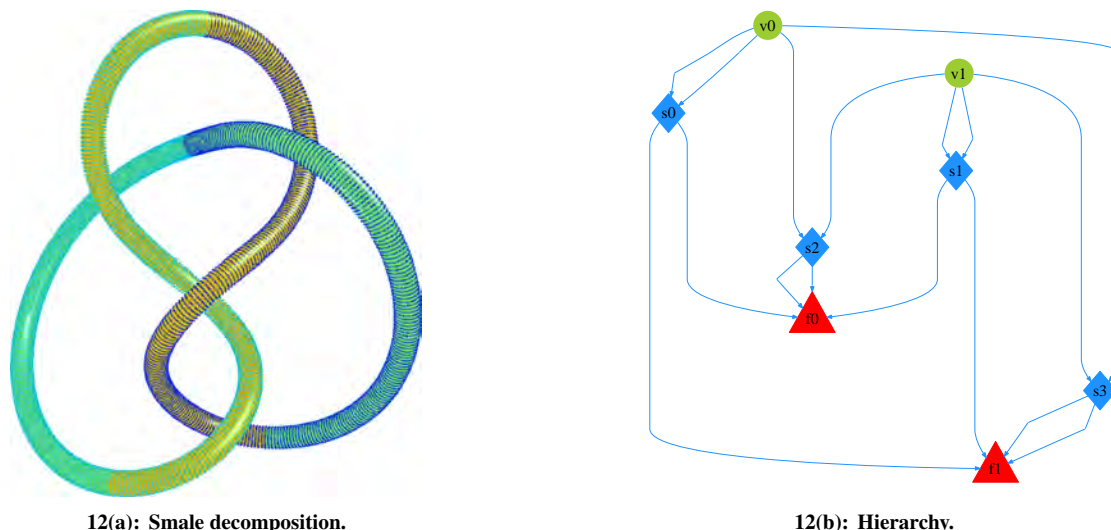
## 5 Experimental results

### (a) Implementation issues

The algorithms presented in section 3 *Computing the Connolly function for a mesh* has been implemented using CGAL. As already mentioned, the data structure used to represent surface triangulations is a halfedge data structure.

The algorithm computing the Connolly function requires a great deal of numerical calculations: computing intersection points between edges and the probe sphere, computing tangent vectors along small circles, evaluating angles and curvatures. All these calculations are performed using `doubles` and we did not observe any significant numerical instability.

The Morse-Smale decomposition algorithm proceeds directly on the halfedge data structure. It requires for each mesh element (vertex, halfedge, facet) a `float` for the scalar field and an additional `void` pointer for the union/find data structure. One halfedge is selected for representing the entire edge. The edges are quick-sorted in an independent array of pointers. The halfedge are marked as visited by an non-null `void` pointer. After the forest creation algorithm, each vertex' (resp. facet) `void` pointer points to the minimum (resp. maximum) of the unstable (resp. stable) region it belongs to. The region's intersection is computed as a `STL set` data structure, whose elements are pairs minimum/maximum, i.e. vertex/facet. Smale's order and cancellation hierarchy are computed by only testing the saddles. The graphs are exported using `graphviz` [3]. The cancellations are stored as pairs minimum/saddle or saddle/maximum. The hierarchy is stored as a `STL priority queue`. One cancellation can invalidate others, Therefore,



12(a): Smale decomposition.

12(b): Hierarchy.

Figure 12: (a) The discrete Morse–Smale decomposition of a figure–eight–knot model with the  $z$ -coordinate as a scalar field. (b) The Smale’s order as a hierarchy of the decomposition of the figure–eight–knot.

the first element of the hierarchy are tested and eventually updated before any cancellation.

In [15], special kinds of saddles, namely monkey saddles, needs to be worked out separately. Those saddles are points whose upper and lower stars contain three or more wedges. With Forman’s framework, those saddles are treated as other ones. More precisely, such an edge is a critical edge whose end vertices belong to separate components of the primal forest, and whose incident faces belong to separate components of the dual forest.

## (b) Experiments

### Experimental setup

The outputs of the decomposition algorithm on several closed surfaces are reported below. In particular, the columns of table 1 read as follows: (i) model name (ii) number of vertices (iii) length of the model bounding box diagonal (iv) Connolly sphere radius (v,vi,vii) number of critical points (Max,saddle,min) (viii) Euler characteristic  $\chi = \sum_c \text{crit.point} \text{index}(c)$  (ix) genus of the surface i.e.  $g = (2 - \chi)/2$ . The calculations presented thereafter required less than a minute on a PC at 1.8 GHz.

From a visual standpoint, a given picture displays the stable, unstable or mixed patches. For such a picture, the patches colors are chosen at random. Consider for example Figure 1(a): each colored patch is a stable manifold and corresponds to a maximum of the Connolly function, namely the red point located at to bottom of the *depression*. Similarly on Figure 1(b), one finds an unstable patch for each maximum of the Connolly function—the blue vertex at the tip of the *knob*. The mixed patches for the same molecule are presented on Figure 1(c) and Figure 15(a)—the latter

being a zoom on a region of the former. The structure of the mixed regions is probably best understood by focusing on the stable and unstable manifolds of the saddles—the green vertices. Each saddle indeed comes with its stable and unstable manifolds which are one-dimensional manifolds. The stable manifold of the saddle consists of the two integral curve starting at minima—the blue vertices—and flowing to the saddle. Similarly, the unstable manifold consists of the two integral curves starting at the saddle and flowing to maxima—the red vertices. Generically, a saddle is therefore at the crossing of four regions. A subtle difference between the smooth and discrete settings is that for the latter, the endpoints of an integral curve may be located at distance one from the critical point on the triangulation—the integral curve may go through one of the one-ring neighbors of the critical point.

### Experiments on molecules

We tested the algorithms on three molecules: a small one—retinal, an enzyme—papain, and a DNA fragment. Retinal is a photo-pigment involved in the capture of photons during photo-synthesis. Papain is a proteolytic enzyme. Of particular interest is the DNA molecule due to the geometry of its two grooves. In each case, the solvent accessible molecular surfaces were produced from a `pdb` file using Michel Sanner’s `msms` software (available from [http://www.scripps.edu/pub/olson-web/people/sanner/html/msms\\_home.html](http://www.scripps.edu/pub/olson-web/people/sanner/html/msms_home.html)), with a probe radius of 1.5 Angstrom.

The results displayed for the three molecules correspond to different radii of the Connolly sphere. As shown on pictures of the retinal molecule, the maxima and minima of the Connolly function indeed correspond to *depressions* and

*knobs*. Some topological noise materializing through tiny patches can be observed at the surface of papain. Getting rid of this noise calls for cancellations as done on Figure 15(b) and Figure 15(c). At last, visual inspection of the DNA molecule is particularly pleasing since the grooves are paved with maxima of the Connolly function.

### Experiments on computer graphics models

We performed additional experiments on standard computer graphics models —see Figure 16(a) and Figure 16(c). The critical points enable one to recover the genus of the surfaces, an overkill process however! More interestingly, the Morse-Smale patches can certainly be useful for the segmentation of surfaces before entering a parameterization or a re-meshing process [13].

## 6 Conclusion

In this paper we invigorated Connolly's function by recasting it into the framework of Morse theory for functions defined over two-dimensional manifolds. Contributions include a careful study of the function for smooth curves and surfaces, an algorithm to evaluate the function on a mesh, an algorithm based upon Forman's discrete Morse theory to construct a discrete Morse-Smale decomposition, as well as experiments on several mesh models. Future work will address the following directions.

On the application side, investigations aiming at reporting the relevance of stable and unstable patches for docking as well as other molecular algorithms are on their way and will be reported elsewhere. From an algorithmic perspective, an interesting contribution would be to be able to perform Morse-Smale decompositions for molecular surface models more accurate than piecewise linear surfaces —e.g. spherical harmonics. The relevance of Morse-Smale diagrams for the general problem of comparing shapes —a ubiquitous problem in computer vision— is also posed. On a more mathematical perspective, several issues deserve investigation. The fact that Connolly's function is close to the mean curvature function is of interest due to the connexion between mean curvature, minimal surfaces and evolution equations. An interesting question is also to check whether or not the Connolly function is generically a Morse function.

### References

[1] R. Forman. A discrete Morse theory for cell complexes. In S. T. Yau, editor, *Geometry, Topology and Physics for Raoul Bott*. International Press, 1995.

[2] R. Forman. Morse theory for cell complexes. *Advances in Mathematics*, 134:90–145, 1998.

[3] E. Koutsofios and S. C. North. Drawing graphs with dot. Technical report, AT&T Bell Laboratories, Murray Hill, NJ, 1993.

	#vces	$\emptyset$	$r$	#M	#s	#m	$\chi$	$g$
retinal	3k	22	1.5	55	97	44	2	0
papaine	17k	81	7	172	335	165	2	0
dna	31k	112	5	218	577	361	2	0
feline	49k	1.88	0.1	477	966	487	-2	2
torus3	4k	231	20	27	81	50	-4	3
fandisk	6k	1.45	0.2	66	122	58	2	0

Table 1: Morse-Smale decompositions: statistics

[4] T. Lewiner, H. Lopes and G. Tavares. Optimal discrete Morse functions for 2-manifolds. *preprint*, 2001.

[5] T. Lewiner, H. Lopes and G. Tavares. Visualizing Forman's discrete vector field. In H.-C. Hege and K. Polthier, editors, *Mathematical Visualization III*. Springer, Berlin, 2002.

[6] S. Smale. Morse inequalities for a dynamical system. *Bulletin of the AMS*, 66:43–49, 1960.

[7] R. E. Tarjan. Efficiency of a good but not linear set union algorithm. *Journal of the ACM*, 22(2):215–225, 1975.

[8] R. E. Tarjan. *Data Structures and Network Algorithms*. Society for Industrial and Applied Mathematics, Philadelphia, 1983.

[9] R. Thom. Sur une partition en cellules associée à une fonction sur une variété. *Comptes Rendus de l'Académie de Sciences*, 228:973–975, 1949.

[10] A. Fomenko and T. Kunii. *Topological Modeling for visualization*. Springer, 1997.

[11] M. Berger and B. Gostiaux. *Géométrie différentielle : variétés, courbes et surfaces (2<sup>nd</sup> edition)*. PUF, 1992.

[12] D. Cohen-Steiner and J.-M. Morvan. Restricted delaunay triangulations and normal cycle. In *Proc. 19th Annu. ACM Sympos. Comput. Geom.*, pages 237–246, 2003.

[13] M. Eck, T. DeRose, T. Duchamp, H. Hoppe, T. Lounsbury and W. Stuetzle. Multiresolution analysis of arbitrary meshes. In *ACM Siggraph*, 1995.

[14] H. Edelsbrunner, M. Facello and J. Liang. On the definition and the construction of pockets in macromolecules. *Discrete Appl. Math.*, 88:83–102, 1998.

[15] H. Edelsbrunner, J. Harer and A. Zomorodian. Hierarchical Morse complexes for piecewise linear 2-manifolds. In *Proc. 17th Annu. ACM Sympos. Comput. Geom.*, pages 70–79, 2001.

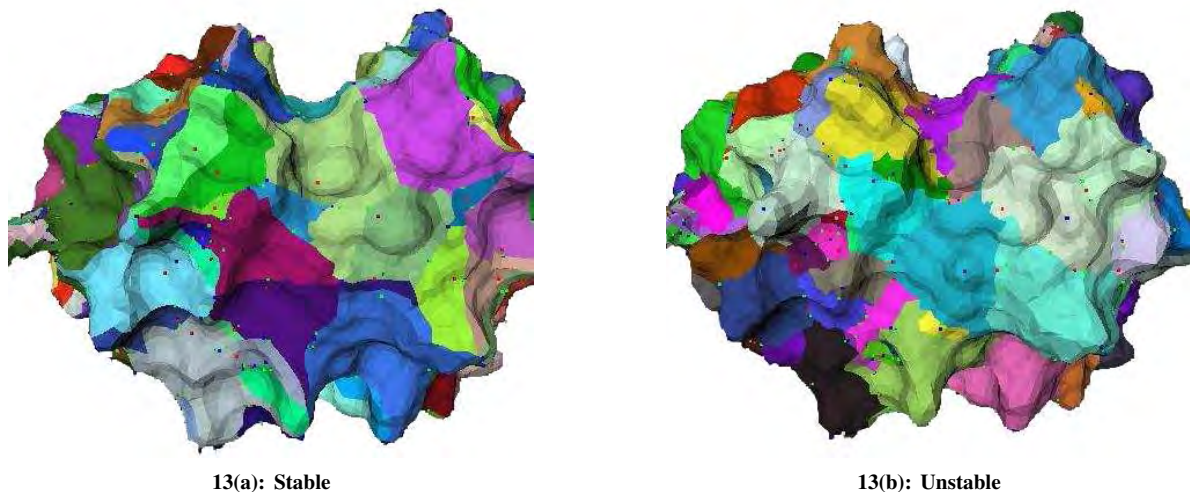
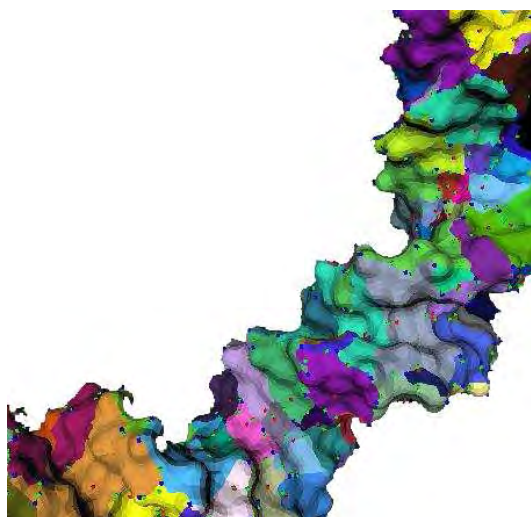
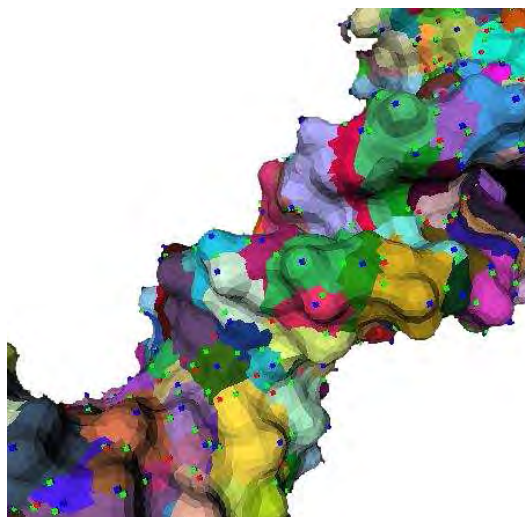


Figure 13: Papain

- [16] F. Cazals and M. Pouget. Estimating differential quantities using interpolating osculating jets. In *Proc. Symp. on Geometry Processing*, 2003.
- [17] J. Giesen and M. John. A dynamical system for disks in the plane. *Preprint*, 2002.
- [18] G. Smith and M. Sternberg. Prediction of protein-protein interactions by docking methods. *Curr. Opin. Struct. Biol.*, 12(1), 2002.
- [19] P. W. Hallinan, G. Gordon, A. Yuille, P. Giblin and D. Mumford. *Two-and Three-Dimensional Patterns of the Face*. A.K.Peters, 1999.
- [20] I. Halperin, B. Ma, H. Wolfson and R. Nussinov. Principles of docking: An overview of search algorithms and a guide to scoring functions. *Proteins*, 47(4), 2002.
- [21] I. Porteous. *Geometric Differentiation (2nd Edition)*. Cambridge University Press, 2001.
- [22] J. Bruce and P. Giblin. *Curves and singularities (2nd Ed.)*. Cambridge, 1992.
- [23] L. Kettner. Designing a data structure for polyhedral surfaces. In *Proc. 14th Annu. ACM Sympos. Comput. Geom.*, pages 146–154, 1998.
- [24] J. W. Milnor. *Morse Theory*. Princeton University Press, Princeton, NJ, 1963.
- [25] M. Connolly. Molecular surfaces: A review. *Network Science*, 14, 1996.
- [26] M. do Carmo. *Differential Geometry of Curves and Surfaces*. Prentice-Hall, 1976.
- [27] M. L. Connolly. Measurement of protein surface shape by solid angles. *J. Mol. Graphics*, 4, 1986.
- [28] M. L. Connolly. Shape complementarity at the hemoglobin a1b1 subunit interface. *Biopolymers*, 25, 1986.
- [29] R. Norel, S. L. Lin, H. Wolfson and R. Nussinov. Shape complementarity at protein-protein interfaces. *Biopolymers*, 34, 1994.
- [30] R. Norel, , H. Wolfson and R. Nussinov. Small molecule recognition: Solid angles surface representation and molecular shape complementarity. *Combinatorial Chemistry & High Throughput Screening*, 2, 1999.
- [31] J. Palis and W. de Melo. *Geometric Theory of Dynamical Systems*. Springer, 1982.
- [32] F. M. Richards. Areas, volumes, packing, and protein structure. *Annu. Rev. Biophys. Bioeng.*, 6:151–176, 1977.
- [33] V. Borrelli, F. Cazals and J.-M. Morvan. On the angular defect of triangulations and the pointwise approximation of curvatures. In *Curves and Surfaces*, St Malo, France, 2002. INRIA Research Report RR-4590.
- [34] W. Cai, M. Zhang and B. Maigret. Protein-ligand recognition using spherical harmonic molecular surfaces: towards a fast and efficient filter for large virtual throughput screening. *J. Molecular Graphics and Modeling*, 53(01):1–16, 2001.

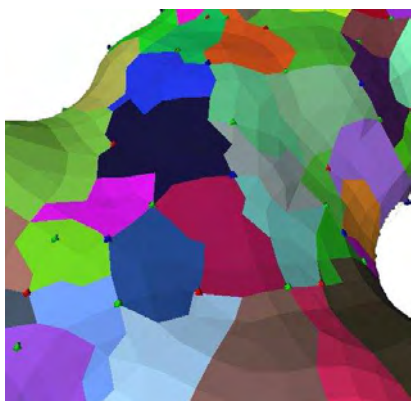


14(a): Stable

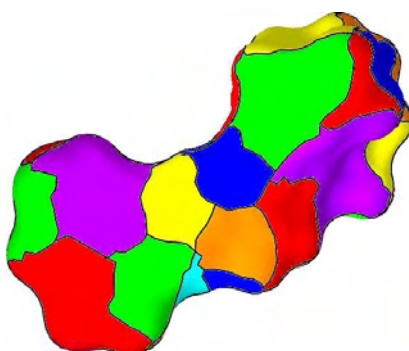


14(b): Unstable

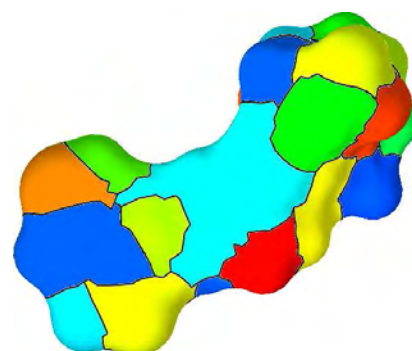
Figure 14: DNA



15(a): Zoom on Morse-Smale regions



15(b): Stable filtered



15(c): Unstable filtered

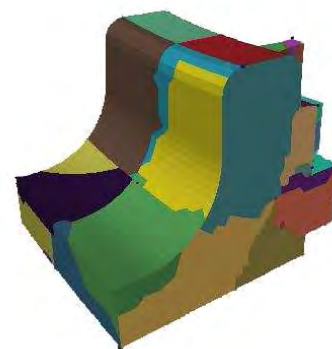
Figure 15: Retinal



16(a): Feline: unstable



16(b): Torus: unstable



16(c): Fandisk:mixed

Figure 16: Classical models